Nonlocal Superelastic Model of Size-Dependent Hardening and Dissipation in Single Crystal Cu-Al-Ni Shape Memory Alloys

Nonlocal Superelastic Model of Size-Dependent Hardening and Dissipation in Single Crystal Cu-Al-Ni Shape Memory Alloys

Lei Qiao,[1] Julian J. Rimoli,[1] Ying Chen,[2] Christopher A. Schuh,[2] and Raul Radovitzky[1,*]

[1]*Department of Aeronautics and Astronautics, Massachusetts Institute of Technology, Cambridge, Massachusetts 02139, USA*
[2]*Department of Materials Science and Engineering, Massachusetts Institute of Technology, Cambridge, Massachusetts 02139, USA*

(Received 2 November 2010; published 24 February 2011; publisher error corrected 28 February 2011)

We propose a nonlocal continuum model to describe the size-dependent superelastic effect observed in recent experiments of single crystal Cu-Al-Ni shape memory alloys. The model introduces two length scales, one in the free energy and one in the dissipation, which account for the size-dependent hardening and dissipation in the loading and unloading response of micro- and nanopillars subject to compression tests. The information provided by the model suggests that the size dependence observed in the dissipation is likely to be associated with a nonuniform evolution of the distribution of the austenitic and martensitic phases during the loading cycle.

DOI: 10.1103/PhysRevLett.106.085504 PACS numbers: 62.20.fg, 62.23.Hj, 62.25.−g

The so-called superelastic effect in shape memory alloys (SMAs) is widely established and has been extensively studied both theoretically and experimentally [1–3]. The superelastic effect is attributed to the stress-induced reversible austenitic-martensitic phase transformation and characterized by the development of significant strains during the transformation which are fully recoverable upon unloading. The hysteresis obtained during a loading cycle corresponds to the energy dissipated during the forward and reverse transformations. Recently, San Juan *et al.* have reported experimental observations of the superelastic effect in Cu-13.7Al-5Ni (wt%) [4] micro- and nanopillars subjected to compressive loading. Their observations exhibit a clear size dependence in damping capacity upon unloading [5,6]. More specifically, their uniaxial compression tests on [001]-oriented Cu-Al-Ni single crystals show that the hysteresis loop in the stress-strain curve for a nanopillar is significantly larger than that for a bulk single crystal. The same size effect is observed in polycrystalline microwire tension experiments for the same alloy [7]. This property makes Cu-Al-Ni SMAs appealing for use in damping applications in microscale and nanoscale devices, or even for integration in fibers and textiles for uses in flexible armor.

In this Letter, we develop a model aimed at describing the mechanical response of this material to help understand the origin of the size-dependent effects. Significant effort has been devoted to developing models for superelastic stress-strain response of SMAs. A comprehensive review may be found in [3]. However, few incorporate size-dependent effects. In [8], the grain-size dependence of the superelastic stress-strain response in bulk polycrystalline Ni-Ti SMAs is modeled via a strain gradient model based on the introduction of an energetic length scale. Other models of SMAs have included nonlocal strain or martensitic volume fraction terms to put a lower bound to the variant size, and avoid numerical problems associated with the nonconvexity of the strain energy function [9,10]. A different phase-field approach has involved a similar consideration [11–13].

In the model presented in this Letter, two internal length scales, an energetic length scale l_e, and a dissipative length scale l_d, are introduced in the free energy and the dissipation rate, respectively, leading to gradient terms on the martensitic volume fraction and its rate of change. The formulation leads to a coupled set of partial differential equations of macroscopic equilibrium and micro-force balance [14–16], whose unknowns are the spatial distribution of the displacement and the martensitic volume fraction. Both equations result from a variational statement of the stationarity of an incremental potential involving the free energy and the dissipation.

Consider a pillar with height h subject to the stress-induced martensitic phase transformation under isothermal condition at temperature θ. The martensitic volume fraction is represented by ξ. For small strains, $u_{,x} = \varepsilon = \varepsilon^e + \xi\varepsilon^t$ where u is the displacement, ε is the total strain, ε^e is the elastic strain, and ε^t is the maximum transformation strain, which is a material constant.

The free energy per unit volume comprises an elastic, a chemical, and a nonlocal term

$$\psi = \frac{1}{2}E(\xi)(\varepsilon - \xi\varepsilon^t)^2 + \frac{\lambda}{\theta_0}(\theta - \theta_0)\xi + \frac{1}{2}S_0 l_e^2(\xi_{,x})^2, \quad (1)$$

where $E(\xi) = \frac{E_a E_m}{E_m + \xi(E_a - E_m)}$ is the effective Young's modulus [17,18], E_a and E_m are the Young's moduli in the pure austenite and martensite, respectively, θ_0 is the equilibrium temperature between the two phases in the stress-free state, and λ is the latent heat. The nonlocal term can be viewed as the interface energy between the two phases. S_0 is a model

parameter with the dimension of stress and l_e is an internal (energetic) length scale.

The introduction of a gradient term on the volume fraction in the free energy results in a separate (microforce) equilibrium equation where the volume fraction is the primary unknown. Consider any segment of the pillar $\{x \in [x_1, x_2] | 0 \le x_1 < x_2 \le h\}$. The internal power in this segment is defined as

$$P^{\text{int}}(\dot{\varepsilon}^e, \dot{\xi}) = \int_{x_1}^{x_2} \sigma \dot{\varepsilon}^e + k\dot{\xi} + k^{\text{nl}} \dot{\xi}_{,x} dx, \tag{2}$$

where $\dot{\times}$ is the rate of variable $\times$, σ is the stress, k and k^{nl} are the work conjugates to the volume fraction ξ and its gradient $\xi_{,x}$, respectively. The external power expended on this segment is defined as

$$P^{\text{ext}}(\dot{u}, \dot{\xi}) = (\hat{t}\,\dot{u} + \hat{k}\,\dot{\xi})|_{x_1}^{x_2}, \tag{3}$$

where $\hat{t}$ and $\hat{k}$ are, respectively, the applied boundary traction and volume fraction force conjugate. At any fixed time τ, the principle of virtual power requires

$$P^{\text{int}}(\dot{\tilde{\varepsilon}}^e, \dot{\tilde{\xi}}) = P^{\text{ext}}(\dot{\tilde{u}}, \dot{\tilde{\xi}}) \tag{4}$$

for any generalized virtual velocity $(\dot{\tilde{u}}, \dot{\tilde{\varepsilon}}^e, \dot{\tilde{\xi}})$ satisfying the kinematic requirement $\dot{\tilde{u}}_{,x} = \dot{\tilde{\varepsilon}}^e + \dot{\tilde{\xi}}\varepsilon^t$. Integration by parts leads to the variational statement

$$0 = -\int_{x_1}^{x_2} \sigma_{,x} \dot{\tilde{u}} dx + \int_{x_1}^{x_2} (k - \sigma\varepsilon^t - k^{\text{nl}}_{,x}) \dot{\tilde{\xi}} dx + [(\sigma - \hat{t})\dot{\tilde{u}}]|_{x_1}^{x_2} + [(k^{\text{nl}} - \hat{k})\dot{\tilde{\xi}}]|_{x_1}^{x_2},$$

which yields

$$\sigma_{,x} = 0, \tag{5}$$

$$k - \sigma\varepsilon^t - k^{\text{nl}}_{,x} = 0, \tag{6}$$

for $x \in (x_1, x_2)$, and $\sigma(x_i, \tau) = \hat{t}(x_i, \tau)$, $k^{\text{nl}}(x_i, \tau) = \hat{k}(x_i, \tau)$, $i = 1, 2$. Equations (5) and (6), are valid for any x_1, x_2 in the admissible range, and, in particular, for the whole pillar ($x_1 = 0$, $x_2 = h$).

Thermodynamic restrictions require that the temporal increase in the free energy should not be greater than the external power expended on the material, i.e.,

$$\dot{\int_{x_1}^{x_2} \psi dx} \le P^{\text{ext}}(\dot{u}, \dot{\xi}). \tag{7}$$

From Eq. (4) it then follows that

$$\dot{\psi} - \sigma\dot{\varepsilon}^e - k\dot{\xi} - k^{\text{nl}}\dot{\xi}_{,x} \le 0 \tag{8}$$

for $x \in (0, h)$. By applying the temporal derivative to the free energy density in Eq. (1) and assuming the elastic response

$$\sigma = E(\xi)(\varepsilon - \xi\varepsilon^t), \tag{9}$$

Eq. (8) is reduced to

$$0 \le \left[k - \frac{1}{2}\frac{\partial E}{\partial \xi}(\varepsilon - \xi\varepsilon^t)^2 - \frac{\lambda}{\theta_0}(\theta - \theta_0)\right]\dot{\xi} + (k^{\text{nl}} - S_0 l_e^2 \xi_{,x})\dot{\xi}_{,x} = \mathcal{D}, \tag{10}$$

where $\mathcal{D}$ is the rate of energy dissipated per unit volume. Inspired by the strain gradient plasticity theories [14–16], k and k^{nl} are defined as follows:

$$k = \frac{1}{2}\frac{\partial E}{\partial \xi}(\varepsilon - \xi\varepsilon^t)^2 + \frac{\lambda}{\theta_0}(\theta - \theta_0) + \frac{Y\dot{\xi}}{\sqrt{(\dot{\xi})^2 + l_d^2(\dot{\xi}_{,x})^2}}, \tag{11}$$

$$k^{\text{nl}} = S_0 l_e^2 \xi_{,x} + \frac{Y l_d^2 \dot{\xi}_{,x}}{\sqrt{(\dot{\xi})^2 + l_d^2(\dot{\xi}_{,x})^2}}, \tag{12}$$

where Y is a model parameter with dimension of stress, and l_d is an internal (dissipative) length scale, which defines the influence of the nonuniform distribution of $\dot{\xi}$ on the dissipation. Indeed, it has been shown in [7] that in small samples of SMA, the surfaces are likely pinning points for the transformation, which tend to suppress the rate of transformation near them, relative to bulk regions away from the surfaces. This provides a possible underlying mechanism for a gradient in $\dot{\xi}$, which in turn gives rise to the dissipative length scale l_d. The dissipation function (per unit volume) then takes the form

$$\mathcal{D} = Y\sqrt{(\dot{\xi})^2 + l_d^2(\dot{\xi}_{,x})^2}, \tag{13}$$

which is nonnegative as required by Eq. (10). It is clear that a nonuniform distribution of $\dot{\xi}$ and larger l_d leads to more dissipation.

The martensitic phase transformation occurs when the thermodynamic driving force associated with the volume fraction reaches some critical value and stays at that value until the transformation is complete [3,19,20]. Inserting Eqs. (11) and (12), in Eq. (6), we obtain

$$\sigma\varepsilon^t - \frac{1}{2}\frac{\partial E}{\partial \xi}(\varepsilon - \xi\varepsilon^t)^2 - \frac{\lambda}{\theta_0}(\theta - \theta_0) + S_0 l_e^2 \xi_{,xx} = \frac{Y\dot{\xi}}{\sqrt{(\dot{\xi})^2 + l_d^2(\dot{\xi}_{,x})^2}} - \frac{\partial}{\partial x}\left[\frac{Y l_d^2 \dot{\xi}_{,x}}{\sqrt{(\dot{\xi})^2 + l_d^2(\dot{\xi}_{,x})^2}}\right], \tag{14}$$

which governs the evolution of the volume fraction ξ. It should be noted that Eq. (14) degenerates to $\sigma\varepsilon^t - \frac{\lambda}{\theta_0} \times (\theta - \theta_0) = \text{sgn}(\dot{\xi})Y$, for $\dot{\xi} \neq 0$, which are the constraints during phase transformation in the local model [20], if ξ and $\dot{\xi}$ are uniform or both internal length scales l_e and l_d are zeros, and $\frac{\partial E}{\partial \xi} = 0$. It is interesting to note from the free energy, Eq. (1), the dissipation, Eq. (13), and the elastic response, Eq. (9), that Eq. (14) can be rewritten as

$$-\left[\frac{\partial \psi}{\partial \xi} - \frac{\partial}{\partial x}\left(\frac{\partial \psi}{\partial \xi_{,x}}\right)\right] = \frac{\partial \mathcal{D}}{\partial \dot{\xi}} - \frac{\partial}{\partial x}\left(\frac{\partial \mathcal{D}}{\partial \dot{\xi}_{,x}}\right),$$

which is the Euler-Lagrange equation of the functional

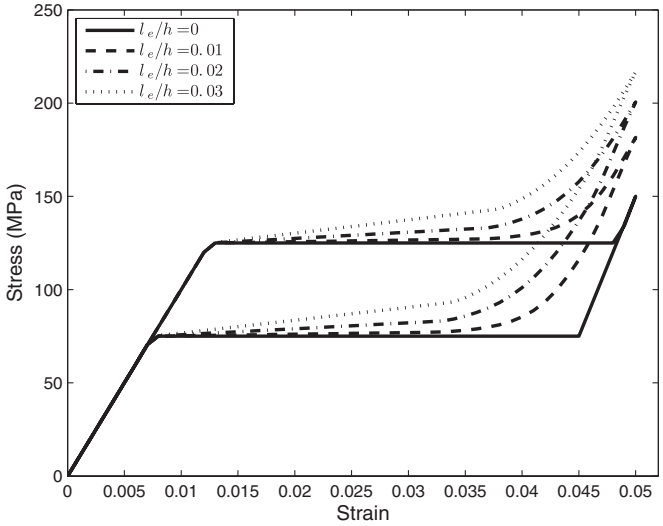

FIG. 1. Stress σ vs macroscopic strain $\hat{u}(t)/h$ for $l_e/h = 0$, 0.01, 0.02, 0.03, $l_d = 0$.

$$J(\dot{\xi}) = \int_0^h \dot{\psi} + \mathcal{D}dx. \tag{16}$$

Replacing the stress σ from Eq. (9) in Eqs. (5) and (14) leads to two coupled partial differential equations governing the displacement $u(x, t)$ and the volume fraction distribution $\xi(x, t)$ with suitable initial and boundary conditions. In our experimental tests, the pillars are assumed to be initially in a stress-free austenitic phase, i.e., $u(x, 0) = 0$, $\xi(x, 0) = 0$ for $x \in [0, h]$. On the boundary, $u(0, t) = 0$, $u(h, t) = \hat{u}(t)$, where $\hat{u}(t)$ is the prescribed displacement, while $\xi(0, t) = \xi(h, t) = 0$ which assumes that the ends of the pillar are obstacles to the martensitic phase transformation. This fully specifies the initial boundary value problem. The resulting equations are solved using a finite element discretization.

The basic model response to compressive loading and unloading cycles is explored for the following parameter values: $E_a = 10$ GPa, $E_m = 15$ GPa, $\varepsilon^t = -0.04$, $\frac{\lambda}{\theta_0}(\theta - \theta_0) = 4$ MPa, $S_0 = 0.1$ GPa, $Y = 1$ MPa, $h = 1$ m. Figure 1 shows a stress-strain cycle fixing $l_d = 0$ and varying $\frac{l_e}{h}$. The solid line corresponds to $\frac{l_e}{h} = 0$ (local model) and exhibits the typical superelastic response of bulk single crystal SMAs. For increasing $\frac{l_e}{h}$, the phase transformation stage exhibits increased hardening, while the critical stress for the forward transformation and the energy dissipation are not affected. During unloading, the reverse transformation starts earlier but ends at the same point. The evolution of the martensitic volume fraction is plotted in Fig. 2 for the case $\frac{l_e}{h} = 0.03$. Because of the boundary constraints, the distribution of the martensitic volume fraction along the pillar is nonuniform during the phase transformation. This nonuniformity is responsible for the smooth transition in the stress-strain curve at the end of the forward transformation and at the beginning of the reverse transformation, in contrast with the sharp changes exhibited by the case of

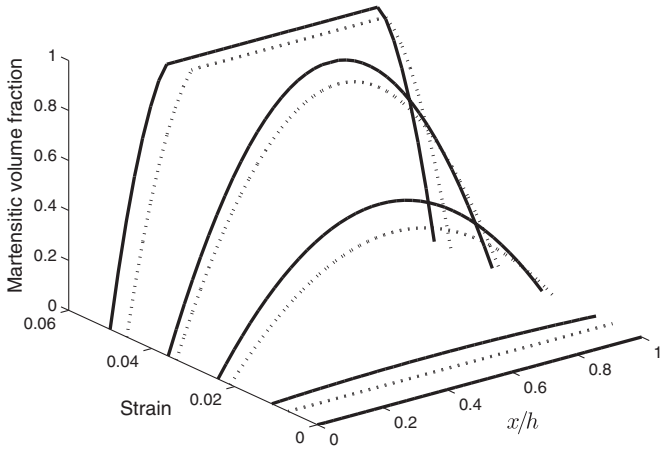

FIG. 2. Evolution of the martensitic volume fraction for $l_e/h = 0.03$, $l_d = 0$ case. Solid lines are used for loading, dashed for unloading.

$\frac{l_e}{h} = 0$. Figure 3 compares the role of the dissipative length scale l_d fixing $l_e = 0$. As $\frac{l_d}{h}$ increases, the gap between the critical stresses for the forward and the reverse transformation also increases, resulting in increased energy dissipation. Figure 4 demonstrates the evolution of the martensitic volume fraction for the case $\frac{l_d}{h} = 0.5$. It differs significantly from Fig. 2, specifically during the unloading part, where at first the reverse transformation occurs everywhere in the pillar, which leads to a sharp change in slope in the stress-strain curve as in the case of $\frac{l_d}{h} = 0$. Close to the end of the reverse transformation, a pure austenitic domain first appears in the center of the pillar and then gradually expands toward the specimen edges, leading to a smooth segment in the stress-strain curve. Subsequently, we explore the model's ability to describe the experimentally observed response of single crystals for three different specimen sizes: (i) bulk single crystal ($h = 9$ mm), (ii) micropillar ($h = 5.1$ μm,

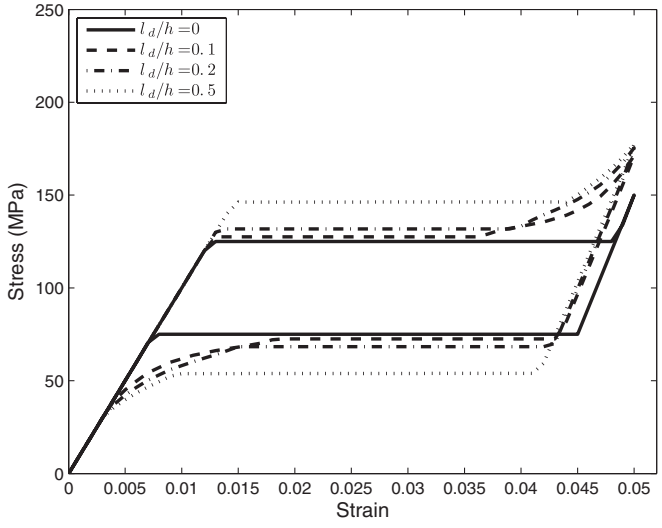

FIG. 3. Stress σ vs macroscopic strain $\hat{u}(t)/h$ for $l_d/h = 0$, 0.1, 0.2, 0.5, $l_e = 0$.

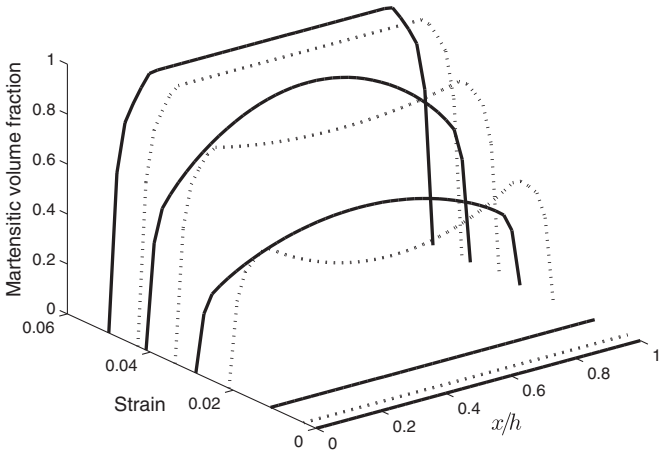

FIG. 4. Evolution of the martensitic volume fraction for the $l_d/h = 0.5$, $l_e = 0$ case. Solid lines are used for loading, dashed for unloading.

diameter 1.7 μm), and (iii) nanopillar ($h = 3.8$ μm, diameter 0.9 μm) [5,6]. The Young's modulus of the austenitic phase, $E_a = 22.1$ GPa, was obtained from the measurement in [6], $E_m = 23.5$ GPa is extracted from the slope of the initial unloading part of the stress-strain curve in case (ii), $\varepsilon^t = -0.05$ is obtained from the calculation in [21]. Other model parameters are calibrated to case (ii), which furnishes the following values: $\frac{\lambda}{\theta_0}(\theta - \theta_0) = 7.6$ MPa, $S_0 = 0.22$ GPa, $Y = 1$ MPa, $l_e = 0.1$ μm, and $l_d = 3.5$ μm. Figure 5 shows the computed (solid) and experimental (circles) stress-strain curves. The model captures a number of features of the response, including the elastic loading and unloading in the two phases, the hardening during the forward and reverse transformation, and the size of the hysteresis loop (dissipation). Considering that temperature changes associated with the transformation were not experimentally available, the thermal stress was held fixed at the calibrated value. This explains the discrepancy in the stress levels predicted for the remaining cases. Regarding the negative slope in the experiment in case (iii), we note that there are explanations available in the literature for some superelastic materials [17], and in the present case

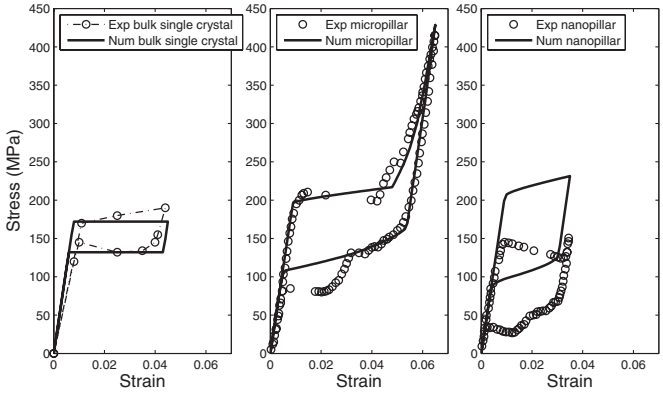

FIG. 5. Simulation of single crystal Cu-Al-Ni compression tests in comparison with experimental results [5,6].

we believe this is an artifact of the mechanical test apparatus, which operates in a condition that is neither exactly load- nor displacement-controlled.

In summary, we presented a nonlocal superelastic model for single crystal SMAs including both an energetic and a dissipative length scales. The agreement with experimental observations suggests that the size-dependent effects in the hardening and energy dissipation of single crystal Cu-Al-Ni SMAs can be attributed to the nonuniform evolution of the martensitic phase arising during the deformation.

The authors acknowledge the support from the U.S. Army through the Institute for Soldier Nanotechnologies, under Contract No. DAAD-19-02-D-0002 with the U.S. Army Research Office.

*rapa@mit.edu

[1] *Shape Memory Materials*, edited by K. Otsuka and C. M. Wayman (Cambridge University Press, Cambridge, England, 1998).
[2] R. Abeyaratne and J. K. Knowles, *Evolution of Phase Transitions: a Continuum Theory* (Cambridge University Press, Cambridge, England, 2006).
[3] D. C. Lagoudas, *Shape Memory Alloys: Modeling and Engineering Applications* (Springer, New York, 2008).
[4] V. Recarte, R. B. Pérez-Sáez, E. H. Bocanegra, M. L. Nó, and J. San Juan, Metall. Mater. Trans. A **33**, 2581 (2002).
[5] J. San Juan, M. L. Nó, and C. A. Schuh, Adv. Mater. **20**, 272 (2008).
[6] J. San Juan, M. L. Nó, and C. A. Schuh, Nanotechnology **4**, 415 (2009).
[7] Y. Chen and C. A. Schuh, Acta Mater. **59**, 537 (2011).
[8] Q. P. Sun and Y. J. He, Int. J. Solids Struct. **45**, 3868 (2008).
[9] J. A. Shaw, Int. J. Solids Struct. **39**, 1275 (2002).
[10] P. Thamburaja and N. Nikabdullah, Comput. Methods Appl. Mech. Eng. **198**, 1074 (2009).
[11] F. Falk, Z. Phys. B **51**, 177 (1983).
[12] Y. Wang and A. G. Khachaturyan, Acta Mater. **45**, 759 (1997).
[13] V. I. Levitas and D. L. Preston, Phys. Rev. B **66**, 134206 (2002).
[14] M. E. Gurtin and L. Anand, J. Mech. Phys. Solids **53**, 1624 (2005).
[15] L. Anand, M. E. Gurtin, S. P. Lele, and C. Gething, J. Mech. Phys. Solids **53**, 1789 (2005).
[16] P. Gudmundson, J. Mech. Phys. Solids **52**, 1379 (2004).
[17] V. A. L'vov, A. A. Rudenko, V. A. Chernenko, E. Cesari, J. Pons, and T. Kanomata, Mater. Trans., JIM **46**, 790 (2005).
[18] V. A. L'vov, C. Picornell, J. Pons, and E. Cesari, Mater. Trans., JIM **46**, 983 (2005).
[19] E. Patoor, D. C. Lagoudas, P. B. Entchev, L. C. Brison, and X. Gao, Mech. Mater. **38**, 391 (2006).
[20] L. Anand and M. E. Gurtin, J. Mech. Phys. Solids **51**, 1015 (2003).
[21] X. Y. Zhang, L. C. Brinson, and Q. P. Sun, Smart Materials and Structures **9**, 571 (2000).